DOI: 10.13009/EUCASS2019-910

Nonlinear system identification for the thermal management of communication satellites

Anıl A. Aksu, Hilmi Sundu, and Erdinç Mermer
*Tübitak Space Technologies Research Institute, Çankaya, Ankara, 06800, Turkey**

In this analysis, we studied nonlinear system identification of the thermal model of the communication satellites. Communication satellites get exposed to external and internal thermal loads during their mission around Earth. The external heat loads include solar flux, albedo flux, and the Earth IR radiation depending on orbit type while the internal loads are the heat dissipation caused by the electrical and mechanical equipments within satellites. Furthermore, the temperature distribution of the satellite equipment has to stay within certain temperature limits to avoid thermal fatigue or overheating of electronic equipments. The control of active heaters and radiators commonly rely on the temperature feedback from real-time thermal simulator. Basically, the thermal simulator solves thermal mathematical model of satellites for the given external and internal heat loads. The thermal mathematical model includes discrete satellite components and discrete radiative and conductive connection between them. These connections are represented as matrices to introduce them to numerical solver in the thermal simulator and, they are formed by various numerical techniques based on the thermal considerations of the problem such as absorptivity, emissivity and conductivity. Moreover, due to the deterioration of multilayer insulation (MLI), the solar flux penetrating into the satellite may significantly increase. As a result, even though these approaches result in good approximation of the thermal mathematical model of satellite, it may include some relatively small error in forming radiation and conduction links. These errors can accumulate in long run and may deviate the result significantly. In this study, we focus on the identification of these errors in aforementioned thermal links between the discrete components of communication satellites and, discuss how the real-time temperature measurement data can be used to improve the quality of the thermal control by means of non-linear system identification.

I. INTRODUCTION

With the development of fast on board computers (OBC), the capability of communication satellites improved considerably. Autonomous on board computers serve both to control various subsystems of satellites and to perform the relevant data processing tasks such as image processing [8]. They remotely communicate with ground stations. These stations retrieve various types of data from satellites [7, 14]. Moreover, these on board computers are also used to simulate the physical processes associated with the control of subsystems such as heat transfer, electrical dissipation. The real-time numerical computation of these physical processes play an important role in both controlling the subsystems of satellites and extending the possible service time of satellites. The real-time simulation of temperature distribution within a satellite is performed by integrating the thermal mathematical model of a given satellite. The thermal mathematical model includes the thermal mass of each discretized finite volume and, conduction and radiation links between them. Moreover, the thermal mathematical models of such satellites are commonly based on computer simulations and subsequent thermal testing. In these simulations, material properties such as conductivity, absorptivity and emissivity are entered manually. These material properties are taken from previous experimental data. However, these datum may include some noise. Moreover, in the computation of radiation links, commonly statistical ray tracing methods are preferred[22]. Even though these methodologies produce a good estimate of the thermal mathematical model of satellites, they may introduce small error. Furthermore, the cyclic heat loads, particularly solar flux, leads to material degradation on MLI outside the satellite, which affects radiation links in the model.

Additionally, the thermal mathematical model is strongly non-linear due to radiation links between the discretized components, therefore it is highly sensitive on the small differences of the physical model[13]. It is particularly evident in diffuse-gray radiation enclosure problems[20]. In the present work, the main focus is on determining these errors associated with conduction and radiation links. In that context, a methodology which uses sparse real

*Electronic mail: anil.aksu@tubitak.gov.tr

time temperature measurements from sensors to identify these errors is described here. The optimal configuration of sensor placement plays an important role in obtaining the required data to identify nonlinear systems. Recent study on the placement of sensors has shown that Singular Value Decomposition (SVD) can be used to identify the appropriate locations[3] by determining most significant singular values. The methodology developed in that study can be applied to general case. For our purposes, Eigendecomposition is also sufficient to obtain these location, as thermal mathematical model for satellites has symmetric and square conduction and radiation matrices. The determination of these sensor locations within a satellite are left for future investigations. Here, two separate thermal mathematical models are generated. The first one is assumed to be the exact model, and artificially generated noise is added to conductance and radiative coupling between discretized finite volumes to form the second model. The temperature distribution obtained by the first model is used as measurement data, and the temperature distribution obtained by the noisy model is used as an initial thermal mathematical model to be updated with the real-time measurement data. The objective of the present study is to identify the actual thermal model by using the real-time measurement data. It requires the identification of critical radiation and conduction links in the thermal network of a model satellite used here.

Several different approaches are taken to identify nonlinear systems[1] which are mostly statistical, however most recent attempts include newly developing machine learning algorithms[17] which are particularly useful for identifying the coefficients of nonlinear partial differential equations. Nonetheless, the thermal mathematical model is discretized version of continuous heat transfer problem of a satellite, the discretization leads to system of nonlinear ordinary differential equations. The main difficulty encountered in such problem is the radiation terms which are dependent on the forth power of the temperature distribution. Additional studies regarding such problems used sparse regression technique to identify a system of nonlinear ordinary differential equations[2, 3]. In the generic form, it can be written as:

$$\frac{\mathrm{d}\vec{X}}{\mathrm{d}t} = \vec{F}(\vec{X}, \vec{\mu}, \vec{f}(t)). \tag{1}$$

where $\vec{X}$ vector represents state variables, $\vec{F}$ is a set of nonlinear functions that govern the problem and $\vec{f}(t)$ is time-dependent forcing vector. The data driven analysis of such non-linear systems is performed by incorporating noisy measurement data[2]. In the analysis, the time series of the measurement data is represented as:

$$\mathbf{X} = \begin{bmatrix} \mathbf{X}^T(t_1) \\ \mathbf{X}^T(t_2) \\ \vdots \\ \mathbf{X}^T(t_m) \end{bmatrix} = \begin{bmatrix} x_1(t_1) & x_2(t_1) & \dots & x_n(t_1) \\ x_1(t_2) & x_2(t_2) & \dots & x_n(t_2) \\ \vdots & \vdots & \ddots & \vdots \\ x_1(t_m) & x_2(t_m) & \dots & x_n(t_m) \end{bmatrix} \tag{2}$$

The similar non-linear dynamical systems such as Lorenz equations are identified by using measurement data using SINDYc algorithm[2, 3]. The dynamical system can be reformulated as sparse regression problem:

$$\dot{\mathbf{X}} = \Theta(\mathbf{X})\Xi + \eta\mathbf{Z}. \tag{3}$$

where $\Theta(\mathbf{X})$ is a library consisting of nonlinear functions of the columns of X and ξ is a sparse vector of coefficients which determines the active terms in the library $\Theta(\mathbf{X})$. Moreover, $\mathbf{Z}$ is modelled as a matrix of independent identically distributed Gaussian entries with zero mean, and noise magnitude η. Similar to the analysis described above, the idea proposed here is to obtain conductivity and radiation matrices from real time measurement during the mission of a communication orbit. In the problem analyzed here, the library consists of $\vec{X}$ and $\vec{X^4}$ terms, as we are dealing with conduction-radiation problem. Furthermore, the main idea is to modify existing conduction and radiation matrices under the assumption that the error in these matrices are small compared to initial value of these matrices. Moreover, the eigenvalue distribution of these matrices provides information about the communication between each finite volume within the satellite. If the eigenvalue of a particular eigenvector in the conduction or the radiation matrix is zero, it physically means that the thermal connection between the components determined by the eigenvector of the matrix that represents a particular physical process does not exist. Therefore, the presence of a noise does not affect these connections. As a result, the sparse regression problem can be reduced to identifying the noise in the non-zero eigenvalues of these matrices. In addition, due to the physical configuration of the problem, the majority of the eigenvalues are zero, which reduces the number of parameters to be identified via sparse regression formulation significantly.

The organization of the manuscript is the following. The thermal model of a communication satellite is analyzed in section II A. In section II B, the sparse regression formulation for the particular problem is discussed. The results

DOI: 10.13009/EUCASS2019-910

are presented in section III. Finally, the limitations and the possible improvement of the methodology are discussed in section IV.

II. ANALYSIS

A. Thermal Model

The physical model includes a continuous satellite components and discrete radiation link between them. The discretization of each component should be able to capture the required detail level to observe and control the temperature change during the mission. In the thermal management of the satellites, the effective heat transfer modes are radiation and conduction. The discretization of these physical processes, conduction and radiation, leads to two separate thermal connectivity matrices which enables to identify the significant thermal links between any of two components. The heat flow between component i and component j via conduction is commonly approximated as[10]:

$$\dot{Q}_{i\to j}^{cond} = \frac{\kappa_{ij} A_{ij} (T_i - T_j)}{L_{ij}}. \tag{4}$$

where κ_{ij} is the conductivity coefficient between ith and jth components, A_{ij} is the effective area and L_{ij} is the effective distance between these components.

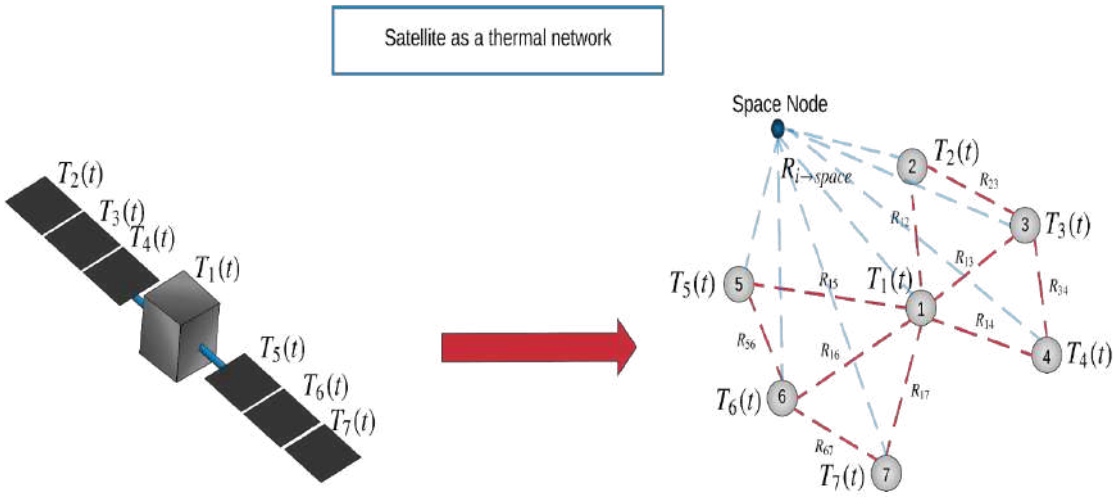

FIG. 1: Illustration of the radiative thermal network of a communication satellite. Typically, a radiative network includes much more points than the illustration, but the network given in the figure shows the important processes that are radiation links between two nodes and radiation links to the space node.

The conduction heat transfer occurs between two adjacent components whereas radiative heat transfer can take place between two component which are not necessarily in physical contact. The heat flow via radiation between surface i and j, to the space from surface i can be given, respectively, as[10]:

$$\dot{Q}_{i\to j}^{rad} = \frac{\sigma(T_i^4 - T_j^4)}{\frac{1-\epsilon_i}{A_i\epsilon_i} + \frac{1-\epsilon_j}{A_j\epsilon_j} + \frac{1}{A_i F_{ij}}}, \qquad \dot{Q}_{i\to s}^{rad} = \sigma\epsilon_i A_i F_{is}(T_i^4 - T_s^4). \tag{5}$$

where σ is Stefan-Boltzmann constant, F_{ij} is the view factor between i^{th} and j^{th} surfaces, A_i is the surface area of i^{th} surface and s subscript stands for the variables related to the space and $T_s = 4K$[11]. The view factor between two surfaces are commonly computed by Monte Carlo ray tracing method[22]. Here, we also use a commercial software which is based on Monte Carlo ray tracing method to generate the initial radiation coupling matrix. As a result, the system of discretized radiation-conduction equations can be given as:

$$[M]\frac{\mathrm{d}\vec{T}}{\mathrm{d}t} = [K]\vec{T} + [R]\vec{T^4} + \dot{\vec{Q}}^{ext}. \tag{6}$$

where $[M]$ is the diagonal thermal mass matrix, $[K]$ is the conductivity matrix and $[R]$ is radiation matrix and $\dot{\vec{Q}}^{ext}$ is the external heating term which includes external heat flow such as solar flux, albedo flux, IR flux and

DOI: 10.13009/EUCASS2019-910

energy dissipation of the electronic components within the satellite. In the particular application, the orbit of the communication satellite is a geostationary orbit(GEO) where albedo and IR fluxes are negligible due to the distance between the satellite and the earth[19]. The computation of the solar flux requires the orientations of both the exterior surfaces and the direction of Sun for computing time varying solar flux on surface. The computation of the direction of Sun vector is explained in Appendix A 1. Additionally, as shown in figure 2, depending on the orientation of Sun direction and the position of the external surfaces, the solar flux on each surface can be reduced by the effect of shadowing, as the external surfaces may block the solar flux incident on other external surfaces. Similar to the computation of the radiation coupling, the shadowing at each time step is computed by Monte Carlo method. The details of the shadowing computation is given in Appendix A 2.

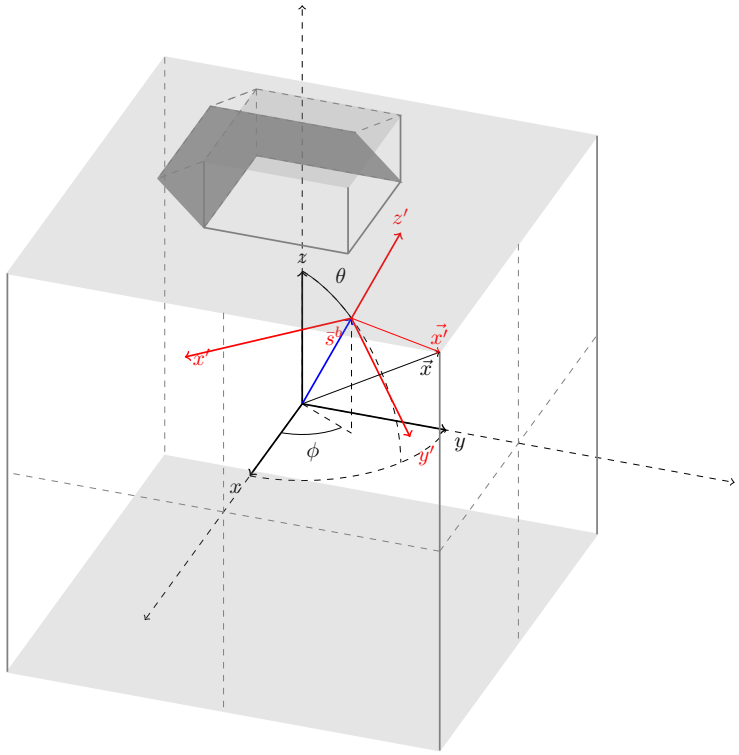

FIG. 2: The direction of Sun vector changes at each time step, so are the orientations of the surfaces with respect to Sun vector. In the figure, Sun vector is denoted as $\hat{z}'$, the other coordinate vectors $\hat{x}'$ and $\hat{y}'$ can be chosen arbitrarily as long as they are orthogonal both to $\hat{z}'$ direction and to each other. Each corner of a given mesh is projected on the plane which has a unit normal in the direction of Sun vector. If a surface has corner points which have z' coordinates higher than those of another surface, and the regions enclosed on x', y' plane by these surfaces' projections overlap, the one with higher z' coordinates shadow some part of the other surface. In the figure, dark shaded area illustrates the area shadowed by the top surface, which is formed by the overlap of the projections mentioned above.

Finally, the energy dissipation of the electronic components are provided by their own model which is beyond the scope of the present study. Consequently, the total external heating can be computed as:

$$\dot{Q}_j^{ext}(t) = \sum_{k=1}^{N_j} \dot{Q}_{jk}^{ext}(t) + \dot{Q}_j^{elec}(t) = \sum_{k=1}^{N_j} \gamma^k(t)\alpha_k S A_k(\bar{n}_k \cdot \bar{s}^{(b)}(t)) + \dot{Q}_j^{elec}(t). \tag{7}$$

where N_j is the number of external surfaces of j^{th} node, S is the solar flux which is typically taken as $1378 W/m^2$[15], α_k is absorptivity coefficient of k^{th} surface, $\bar{n}_k$ is the unit normal of k^{th} surface, A_k is the surface area of k^{th} surface, $\gamma^k(t)$ is the time-dependent ratio of unshadowed part of k^{th} surface, $\bar{s}^{(b)}(t)$ is Sun vector with respect to the satellite centred coordinate system and $\dot{Q}_j^{elec}(t)$ is the heat load due to electrical dissipation in j^{th} node. After computing associated matrices and external heat flows, the temperature distribution of the satellite is advanced in time by the classical forth order Runge-Kutta time integration scheme[4].

DOI: 10.13009/EUCASS2019-910

B. Nonlinear System Identification

As mentioned earlier, the thermal mathematical model is formed under simplifying assumptions and approximations, therefore it includes some error in $[K]$, $[R]$ and possibly $[M]$. However, in most cases, the diagonal thermal mass matrix $[M]$ can be experimentally obtained more accurately[5] than $[K]$ and $[R]$ matrices. In this study, we focus primarily on identifying errors in $[K]$ and $[R]$ matrices, as they are likely to build up and cause considerable error in the computation of temperature distribution within the model satellite. However, errors in conduction and radiation matrices does not affect the sparsity pattern of these matrices. As the form of these matrices are dependent on the communication between nodes which represent finite volume discretization of a model satellite, if a radiation or conduction link does not exist between two nodes, a modelling or measurement noise can not establish such a link. Therefore, these noises only affect the existing thermal links.

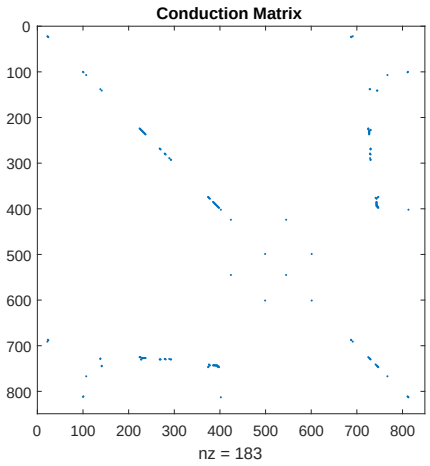

(a) The form of a conduction matrix for a model satellite

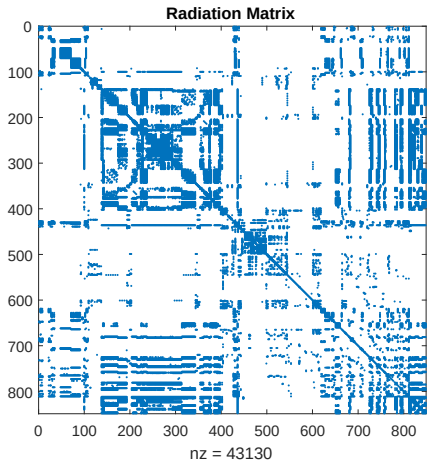

(b) The form of a radiation matrix for a model satellite

FIG. 3: Sparsity pattern of conduction and radiation matrices for a model satellite, which have large number of zero eigenvalues.

As a result, the presence of noises does not affect the sparsity patterns of the conduction matrix shown in figure 3a and the radiation matrix shown in figure 3b. Furthermore, the existing conduction and radiation links can be identified by Eigendecomposition of these matrices. Basically, these links are eigenvectors with nonzero eigenvalues in these matrices. Moreover, since both of these matrices are symmetric, their eigenvectors are mutually orthogonal[21]. Therefore, these matrices can be decomposed as:

$$[K] = \sum_{k=1}^{N_{eig}^{c}} \lambda_k^c \mathbf{e}_k^c \otimes \mathbf{e}_k^c, \qquad [R] = \sum_{k=1}^{N_{eig}^{r}} \lambda_k^r \mathbf{e}_k^r \otimes \mathbf{e}_k^r \tag{8}$$

where c superscript denotes terms associated with the conduction matrix, r superscript denotes terms associated with the radiation matrix, $\otimes$ stands for outer product of vectors, N_{eig} is number of nonzero eigenvalues, λ_k is k^{th} eigenvalue and $\mathbf{e}_k$ is k^{th} eigenvector.

The decomposed forms of conduction and radiation matrices give an important insight about how heat flow is distributed between nodes. In the absence of external heating, eigenvectors with eigenvalues which have higher absolute values dominate the temperature distribution in long run. Therefore, these eigenvectors point out more effective conduction and radiation links between nodes. As a result, noise in the corresponding eigenvalues may result in considerable error in temperature distribution. Furthermore, as mentioned earlier, modelling noise does not affect trivial eigenvalues, as the thermal links determined by the corresponding eigenvector physically does not exist. For example, the radiative thermal links within the satellite is independent of the radiative thermal links of the external surfaces. Consequently, regression problem here is restricted to the thermal links with nonzero eigenvalues. It significantly reduces the computational effort, as most of eigenvalues of these matrices are zero.

In a classical regression problem, data samples in $\mathbb{R}^n$ are supposed to be represented by a linear combination of a set of linearly independent vectors $S = \{\mathbf{v}_1, \mathbf{v}_2, ...\mathbf{v}_m, \}$ where $m < n$ by minimizing L_2 norm of error[4]. If $m = n$, the set S spans the entire space, therefore it causes overfitting problem. In previous studies, overfitting problem was solved by obtaining measurement form several consequent time steps as represented in equation 2[2, 3]. In the

present study, overfitting problem can be handled by using only the eigenvectors with nonzero eigenvalues. As a result, data from a single time step is sufficient to overcome overfitting problem. However, regression coefficients obtained from a single step may not be sufficient, as some of existing thermal links might not have been active until that time step and they may become effective at following time steps.

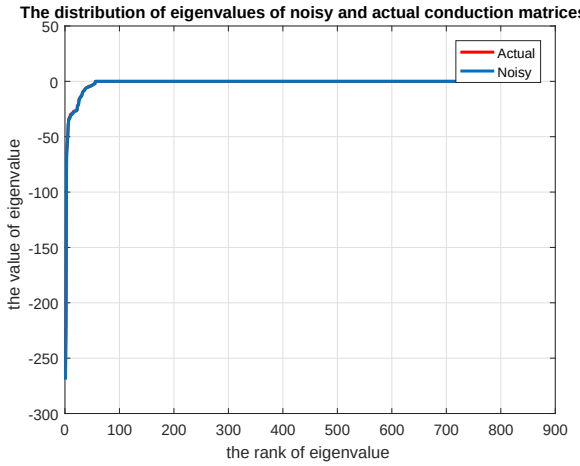

(a) The distribution of eigenvalues of noisy and actual conduction matrices

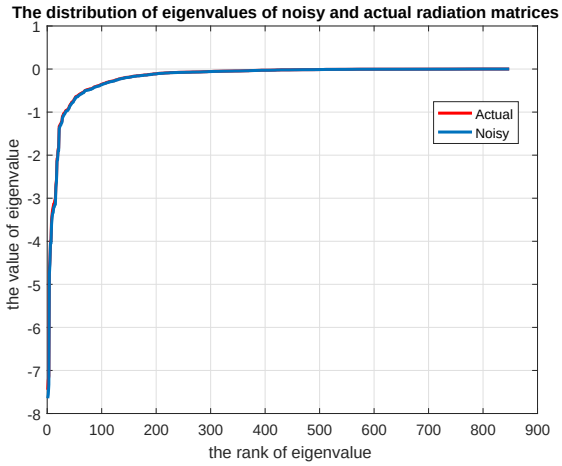

(b) The distribution of eigenvalues of noisy and actual radiation matrices

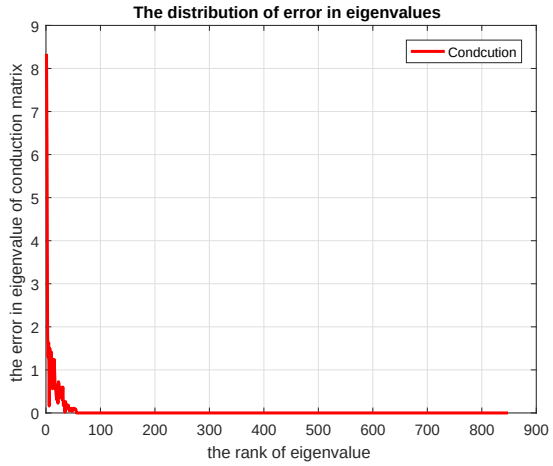

(c) Error in eigenvalues of conduction matrix due to the presence of noise

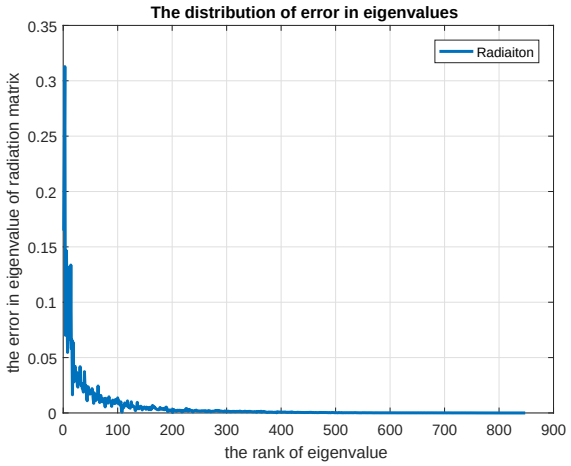

(d) Error in eigenvalues of radiation matrix due to the presence of noise

FIG. 4: The distribution and error in eigenvalues of conduction and radiation matrices

As shown in figure 4a, after the first 100 eigenvalues of conduction matrix, the rest of them are zero. Similarly, after the first 300 eigenvalues of radiation matrix, the rest of them are zero as shown in figure 4b. The number of significant eigenvalues are larger in radiation matrix, as there are more active radiation links available than conduction links. Taking these into account, the conduction-radiation problem formulated in equation 6 can be updated as:

$$[M]\frac{\mathrm{d}\vec{T}}{\mathrm{d}t} = ([K] + [\Delta K])\vec{T} + ([R] + [\Delta R])\vec{T^4} + \dot{\vec{Q}}^{ext}. \tag{9}$$

where $[K]$ is the initial conduction matrix , $[\Delta K]$ is an update matrix to be added to the initial conduction matrix, $[R]$ is the initial radiation matrix, $[\Delta R]$ is an update matrix to be added to the initial radiation matrix. These update matrices are used to converge the actual configuration of the thermal links within the satellite. These update matrices can be given as:

$$[\Delta K] = \sum_{k=1}^{N^c_{eig}} \beta^c_k \lambda^c_k \mathbf{e}^c_k \otimes \mathbf{e}^c_k, \qquad [\Delta R] = \sum_{k=1}^{N^r_{eig}} \beta^r_k \lambda^r_k \mathbf{e}^r_k \otimes \mathbf{e}^r_k \tag{10}$$

where β^c_k and β^r_k are update coefficients of the significant eigenvalues of radiation and conduction matrices. In the following step, the error vector can be computed by the difference between the measurement temperature distribution

and the temperature obtained by the initial model. Therefore, the error vector can be given as:

$$\vec{e} = [M]\frac{\vec{T}^{meas}_{n+1} - \vec{T}_{n+1}}{\Delta t} - [\Delta K]\vec{T}_n - [\Delta R]\vec{T^4}_n \neq 0. \tag{11}$$

The regression problem here is to minimize L_2 norm of error vector. Hereafter, $\vec{e} = \mathbf{e}$ and $\vec{T} = \mathbf{T}$. By substituting Eigendecomposition of $[\Delta K]$ and $[\Delta R]$, the regression problem can be alternatively given as:

$$\min_{(\beta^c_k,\beta^r_k)\in\mathbb{R}} \left\| b - (\sum_{k=1}^{N^c_{eig}} \beta^c_k \lambda^c_k \mathbf{e}^c_k \otimes \mathbf{e}^c_k)\mathbf{T}_n - (\sum_{k=1}^{N^r_{eig}} \beta^r_k \lambda^r_k \mathbf{e}^r_k \otimes \mathbf{e}^r_k)\mathbf{T}^4_n \right\|_2 . \tag{12}$$

where $b = [M]\frac{\mathbf{T}^{meas}_{n+1} - \mathbf{T}_{n+1}}{\Delta t}$. Under the formulation given in equation 12, the inner product of error vector by itself can be minimized to solve the regression problem. The minimization of the inner product of error vector by itself can be formulated as:

$$\frac{\partial(\mathbf{e}^T\mathbf{e})}{\partial\beta^c_i} = 0, \qquad \frac{\partial(\mathbf{e}^T\mathbf{e})}{\partial\beta^r_i} = 0. \tag{13}$$

where T superscript stands for transpose operation. Explicitly, these relations can be given as:

$$\begin{aligned} &\lambda^c_i(\mathbf{T}^T_n\mathbf{e}^c_i)(\mathbf{e}^c_i)^T(b - (\sum_{k=1}^{N^c_{eig}} \beta^c_k \lambda^c_k \mathbf{e}^c_k \otimes \mathbf{e}^c_k)\mathbf{T}_n - (\sum_{k=1}^{N^r_{eig}} \beta^r_k \lambda^c_k \mathbf{e}^c_k \otimes \mathbf{e}^r_k)\mathbf{T}^4_n) = \\ &\lambda^c_i(\mathbf{T}^T_n\mathbf{e}^c_i)(((\mathbf{e}^c_i)^T b) - \beta^c_i\lambda^c_i((\mathbf{e}^c_i)^T\mathbf{T}_n) - (\sum_{k=1}^{N^r_{eig}} \beta^r_k\lambda^r_k((\mathbf{e}^c_i)^T\mathbf{e}^r_k)((\mathbf{e}^r_k)^T\mathbf{T}^4_n))) = 0. \end{aligned} \tag{14}$$

$$\begin{aligned} &\lambda^r_i((\mathbf{T}^4_n)^T\mathbf{e}^r_i)(\mathbf{e}^r_i)^T(b - (\sum_{k=1}^{N^c_{eig}} \beta^c_k \lambda^c_k \mathbf{e}^c_k \otimes \mathbf{e}^c_k)\mathbf{T}_n - (\sum_{k=1}^{N^r_{eig}} \beta^r_k \lambda^c_k \mathbf{e}^c_k \otimes \mathbf{e}^r_k)\mathbf{T}^4_n) = \\ &\lambda^r_i((\mathbf{T}^4_n)^T\mathbf{e}^r_i)(((\mathbf{e}^r_i)^T b) - (\sum_{k=1}^{N^c_{eig}} \beta^c_k\lambda^c_k((\mathbf{e}^r_i)^T\mathbf{e}^c_k)((\mathbf{e}^c_k)^T\mathbf{T}_n) - \beta^r_i\lambda^r_i((\mathbf{e}^r_i)^T\mathbf{T}^4_n))) = 0. \end{aligned} \tag{15}$$

The set of equations described above determines β^c_i and β^r_i coefficients. The solution of the system above can be done by standard linear solvers such as GMRES method or LU decomposition[21], however one of the possible problems associated with the solution described above is the high condition number of the system, if it is left in the form presented in equation 14 and equation 15.

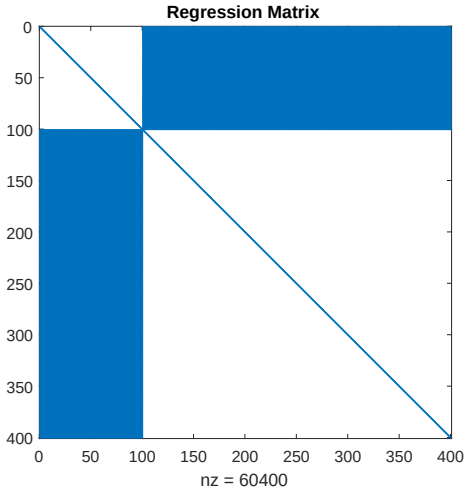

FIG. 5: The form of regression matrix described in equation14 and equation 15.

The main cause of high condition number problem is that temperature distribution within the satellite is in $\mathcal{O}(10^2K)$, and radiation terms are in $\mathcal{O}(T^4)$ whereas conduction terms are in $\mathcal{O}(T)$, resulting in large scale difference between the upper part and the lower part of the regression matrix shown in figure 5. Nonetheless, the conditioning

problem can be improved if factors $\lambda_i^c(\mathbf{T}_n^T\mathbf{e}_i^c)$ and $\lambda_i^r((\mathbf{T}_n^4)^T\mathbf{e}_i^r)$ are eliminated. Therefore, the set of equations can be alternatively given as:

$$\beta_i^c\lambda_i^c((\mathbf{e}_i^c)^T\mathbf{T}_n) + (\sum_{k=1}^{N_{eig}^r}\beta_k^r\lambda_k^r((\mathbf{e}_i^c)^T\mathbf{e}_k^r)((\mathbf{e}_k^r)^T\mathbf{T}_n^4)) = ((\mathbf{e}_i^c)^T b), \tag{16}$$

$$(\sum_{k=1}^{N_{eig}^c}\beta_k^c\lambda_k^c((\mathbf{e}_i^r)^T\mathbf{e}_k^c)((\mathbf{e}_k^c)^T\mathbf{T}_n) + \beta_i^r\lambda_i^r((\mathbf{e}_i^r)^T\mathbf{T}_n^4)) = ((\mathbf{e}_i^r)^T b). \tag{17}$$

After solving the system above, the eigenvalues of both conduction and radiation matrices can be modified as:

$$(\lambda_i^c)^{n+1} = (1+\beta_i^c)(\lambda_i^c)^n, \qquad (\lambda_i^r)^{n+1} = (1+\beta_i^r)(\lambda_i^r)^n. \tag{18}$$

where n represents the number of updates. If an update is required can be checked by L_2 norm of error. Depending on the required accuracy, a threshold value for error bound can be determined. Regardless of updated eigenvalues, corresponding eigenvectors remain the same for entire identification process.

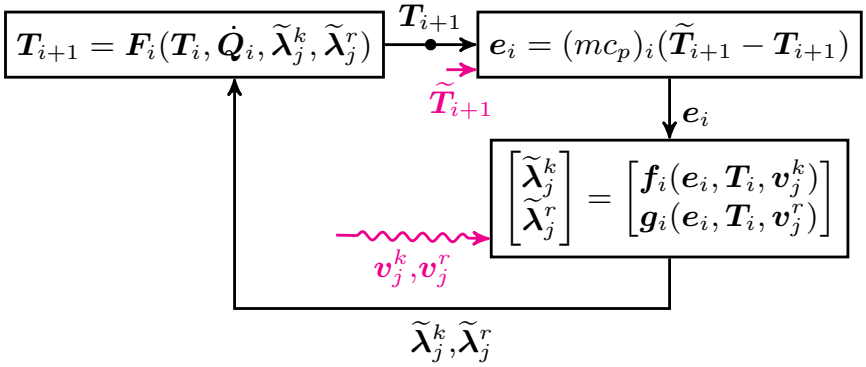

FIG. 6: Nonlinear system identification algorithm diagram: Existing thermal model calculates temperature distribution, then the difference between temperature distribution from measurements which is shown as $\widetilde{\mathbf{T}}_{i+1}$ and the calculated temperature distribution is computed and multiplied with the corresponding thermal mass, finally the resultant product and eigenvectors of initial matrices, $\mathbf{v}_j^k$ and $\mathbf{v}_j^r$, are send to the regression algorithm to compute updates of eigenvalues of radiation and conduction matrices.

Furthermore, the nonlinear system identification algorithm described in figure 6 is more effective, when it is used after certain amount of time steps. As errors accumulate, the algorithm can capture noise more effectively. The identification process may be required more than once, depending on external heat flow profile some existing thermal links might not have been active. But, on latter stages of a mission of satellite, these thermal links may start transferring heat flow. Therefore, their error may become more apparent on advancing stages of the mission. Moreover, towards the end of life time, the surface properties may deteriorate and result in a change in radiation and conduction matrices. Consequently, it is more feasible to control error at certain stages of the mission.

III. RESULTS

The numerical methods described above deals with the thermal mathematical modelling of a communication satellite and the associated nonlinear system identification problem. The thermal mathematical model of a communication satellite includes thermal mass of discretized finite volumes, conduction and radiation matrices. Moreover, during a mission around a geosynchronous orbit, the solar flux changes transiently with respect to the position of a satellite. The amount heat flow on each external surface is dependent on its unit normals orientation with respect to Sun vector.

Another consideration associated with the heat flow on each surface due to solar flux is the shadowing effect. The orientation of each surface with respect to each and Sun vector may block heat flow on some of the external surfaces. As a result, the rate of shadowing is highly dependent on the position of satellite during a cycle around its orbit. As described in detail in Appendix A 2, the ratio of the area which gets exposed to the solar flux varies at each

surface. The total heat flow on each surface is computed both with the effect of shadowing and without the effect of shadowing. The result of both configuration is given in figure 7a. The difference between the heat flow in each configuration which is shown in figure 7b shows that it significantly reduces the amount of heat flow on some surface, thus the overall temperature distribution.

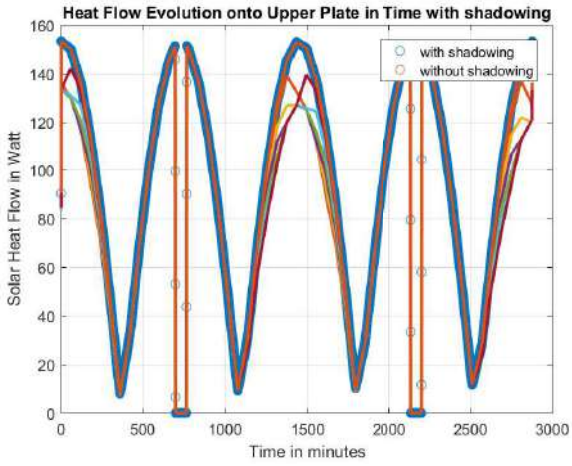

(a) Heat flow on external surfaces during a cycle around a geosynchronous orbit.

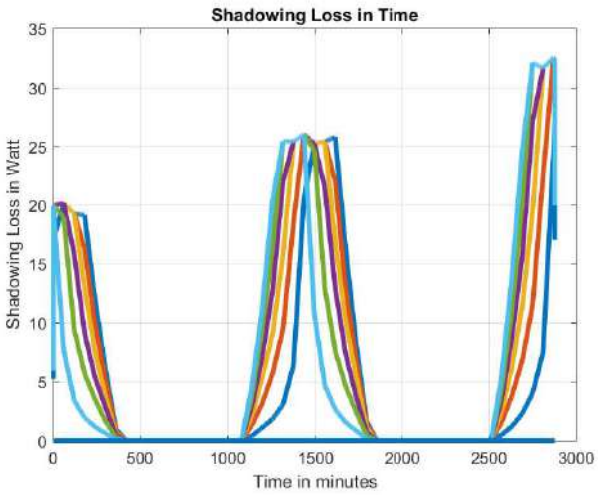

(b) Heat flow loss due to the shadowing effect.

FIG. 7: The heat flow on external surfaces of a communication satellite under the shadowing effect.

Inevitably, the rate of heat flow changes the temperature distribution of the satellite considerably. The transient evolution of the temperature variation of the model satellite is given in figure 8a. In the results presented in figure 8a, a model assumed to be the actual thermal mathematical model is advanced in time under the solar flux with the shadowing effect.

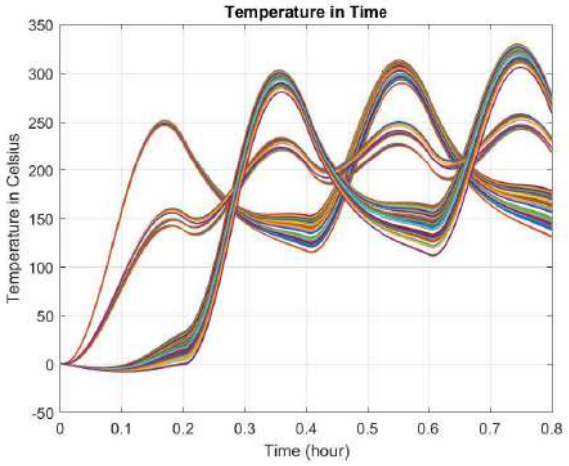

(a) Temperature distribution of a actual model of a communication satellite

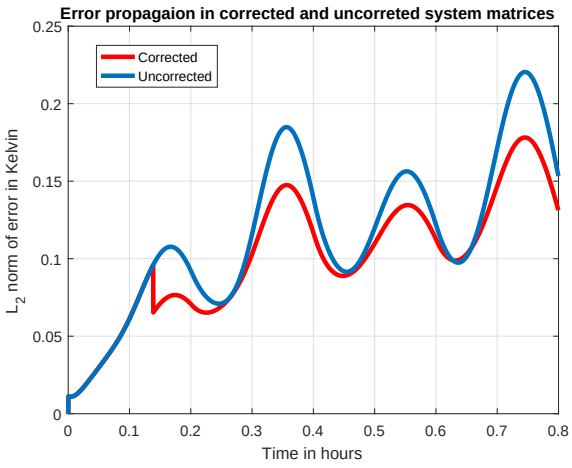

(b) The propagation of error due to presence of noise in both corrected and uncorrected model with nonlinear system identification algorithm

FIG. 8: The evolution of the temperature distribution of an actual model and the propagation of noise in both corrected and uncorrected models.

As mentioned earlier, an additional model to which noise added is generated and it is also advanced in time. After 500 time steps, the error vector is used to identify the updates of eigenvalues of conduction and radiation matrices. The corrected model is advanced in time to observe its effect on error propagation. As shown in figure 8b, the identification decreases the error considerably.

DOI: 10.13009/EUCASS2019-910

IV. CONCLUSION

In this present study, the objective is to develop a numerical model which can analyse heat transfer problem in satellite. The heat transfer modes in satellite are radiation which enables to transfer heat between components of the satellite and also with outer space. In detail, the heat transfer with outer space includes net heat flux from sun which varies based on satellite's location and radiative heat loss form all surfaces. In addition, conductive heat transfer mode occurs within each component whereas the conduction between components are negligible.

The physical model is one aspect of the problem, another issue to be addressed is to introduce these heat transfer modes to computer. First, the system is written as thermal mass matrix which is multiplied with the time derivative of the system. Moreover, the conduction is discretized and written in terms of conduction connectivity matrix. The radiation is also discretized and given as radiation matrix. The modelling noise in these matrices may lead to considerable accumulation error.

In the present study, the main objective is to minimize the error caused by noise in the modelling of the thermal mathematical model of a communication satellite. A general framework is presented here. However, the algorithm described above still lacks data augmentation of temperature measurements. The future extension of the current study may deal with the associated measurement data insufficiency and optimal sensor placement.

A. Data insufficiency problem and optimal sensor placement

The real-time temperature measurement is limited to certain locations, therefore there are missing temperature measurement data. However, the computed temperature distribution and these measurement data can be used to augment the measurements. The measurement data and the computed data at each time step can also be stored as a vector with missing components as:

$$\mathbf{T}_{meas} = \begin{bmatrix} T^1_{meas} \\ T^2_{meas} \\ T^3_{missing} \\ T^4_{missing} \\ \vdots \\ T^n_{meas} \end{bmatrix}, \quad \mathbf{T}_{comp} = \begin{bmatrix} T^1_{comp} \\ T^2_{comp} \\ T^3_{comp} \\ T^4_{comp} \\ \vdots \\ T^n_{comp} \end{bmatrix} \tag{19}$$

The error due to modelling can be computed as:

$$\eta = \begin{bmatrix} \frac{T^1_{meas} - T^1_{comp}}{\Delta T^1_{comp}} \\ \frac{T^2_{meas} - T^2_{comp}}{\Delta T^2_{comp}} \\ \vdots \\ \frac{T^n_{meas} - T^n_{comp}}{\Delta T^n_{comp}} \end{bmatrix} \tag{20}$$

η_i are independent and identically distributed (i.i.d.) errors taken from a zero-mean, Gaussian distribution with variance σ_η. Given this assumed noise distribution, the probability of observing the value u^1_i can be modelled as:

$$f_\eta(u^1_i \mid f_i(\theta)) = \frac{1}{\sqrt{2\pi\sigma_\eta}} e^{-\frac{1}{2\sigma^2_\eta}((u^1_i - f_i(\theta))^2}. \tag{21}$$

Equation 21 includes the effects of uncertainty due to measurement and noise. Bayesian inference is well-suited for such data augmentation problem. In generic definition, prior, likelihood and posterior distribution can be related as:

$$f(\theta \mid X) = \frac{f(\theta) f(X \mid \theta)}{f(X)} \tag{22}$$

where $f(X) = \int f(\theta) f(X \mid \theta) \mathrm{d}\theta$, $f(\theta)$ is the prior, $f(\theta \mid X)$ is the posterior and $f(X \mid \theta)$ is the likelihood distributions. Bayesian approach can be taken to get better estimates of associated coefficients used here like conductivity and radiation matrices[6, 9].

Acknowledgments

Authors wish to thank Altuğ Okan, Ömer Refik Sözbir and Barış Mıhçak for their commentary on the early version of the manuscript and insightful discussions.

DOI: 10.13009/EUCASS2019-910

APPENDIX A: SOLAR FLUX CALCULATION

1. The computation of the Sun direction with respect to the satellite coordinate axis

For stationary components of a communication satellite, the unit normals with respect to satellite centred coordinate system of external surfaces are fixed for an entire mission. Therefore, it is computationally less demanding to determine the direction of Sun vector with respect to satellite centred coordinate system rather than the unit normals of each surface with respect to Earth centred coordinate at each time step.

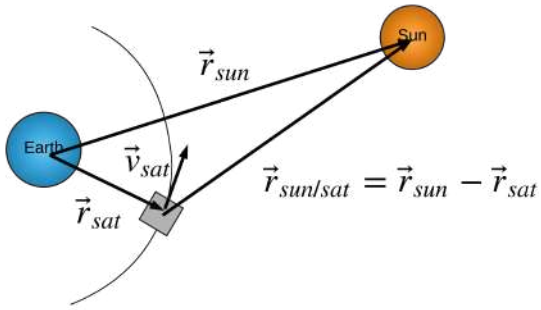

(a) As shown in the figure, $\vec{r}_{sun}$ is the position of Sun with respect to Earth centred coordinate system, and $\vec{r}_{sun}$ is the position of the satellite with respect to Earth centred coordinate system, therefore the position of Sun with respect to the satellite is given as $\vec{r}_{sat/sun} = \vec{r}_{sun} - \vec{r}_{sat}$.

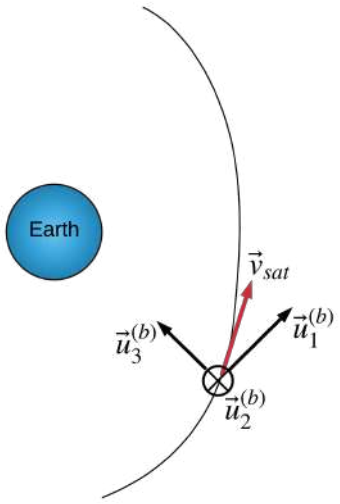

(b) In the figure, $\vec{u}_1^{(b)}$, $\vec{u}_2^{(b)}$ and $\vec{u}_3^{(b)}$ show the unit normal directions of the satellite, and $\vec{v}_{sat}$ shows the velocity vector of the satellite.

FIG. 9: The schematic representation of the position vectors of Sun and a satellite with respect to Earth centred coordinate system.

The unit normals of the satellite shown in figure 9b can be computed as follows:

$$\vec{u}_3^{(b)} = \frac{-\vec{r}_{sat}}{\|\vec{r}_{sat}\|}, \quad \vec{u}_2^{(b)} = \frac{\vec{u}_3^{(b)} \times \vec{v}_{sat}}{\left\|\vec{u}_3^{(b)} \times \vec{v}_{sat}\right\|}, \quad \vec{u}_1^{(b)} = \frac{\vec{u}_2^{(b)} \times \vec{u}_3^{(b)}}{\left\|\vec{u}_2^{(b)} \times \vec{u}_3^{(b)}\right\|} \tag{A1}$$

In total, the satellite's orientation can be given as:

$$\hat{C}^{(i,b)} = \left[\bar{u}_1^{(b/i)} \quad \bar{u}_2^{(b/i)} \quad \bar{u}_3^{(b/i)}\right] \tag{A2}$$

where i subscript represents the unit vectors of the satellite centred coordinate system with respect to Earth centred coordinate system. After forming the transformation matrix $\hat{C}^{(i,b)}$, an arbitrary $\bar{x}^b$ vector can be transformed into the Earth centred coordinates as follows:

$$\bar{x}^i = \hat{C}^{(i,b)} \bar{x}^b. \tag{A3}$$

where $\bar{x}^i$ represents the transformation of $\bar{x}^b$ with respect to the Earth centred coordinate system. Ultimately, Sun vector with respect to the satellite centred coordinate system can be given as:

$$\bar{r}^b_{sun/sat} = (\hat{C}^{(b,i)})^T \bar{r}^i_{sun/sat}. \tag{A4}$$

Finally, it is normalized as:

$$\bar{s}^{(b)} = \frac{\bar{r}^b_{sun/sat}}{\left\|\bar{r}^b_{sun/sat}\right\|} \tag{A5}$$

DOI: 10.13009/EUCASS2019-910

2. Shadowing of the solar flux

The solar flux from the sun comes from long enough distance that it can be assumed planar heat flux. In the closer source of heat flux, typically Monte Carlo methods are preferred [12, 16]. In the case of planar source, the shadowing issue can be much easily solved and it is computationally less expensive. The shadowing for the planar source of rays can be basically computed by projection on 2-D plane where the solar flux is incident onto the satellite. The projection of each component can be computed by the rotation of the plane with respect to the direction of the unit normal of the sun as follows:

$$\begin{bmatrix} \cos\theta & 0 & \sin\theta \\ 0 & 1 & 0 \\ -\sin\theta & 0 & \cos\theta \end{bmatrix} \begin{bmatrix} \cos\phi & \sin\phi & 0 \\ -\sin\phi & \cos\phi & 0 \\ 0 & 0 & 1 \end{bmatrix} \begin{bmatrix} x \\ y \\ z \end{bmatrix} = \begin{bmatrix} x' \\ y' \\ z' \end{bmatrix}. \tag{A6}$$

After the projection operation described in equation A6, the projection on $x' - y'$ plane can be used to compute the rate of shadowing.

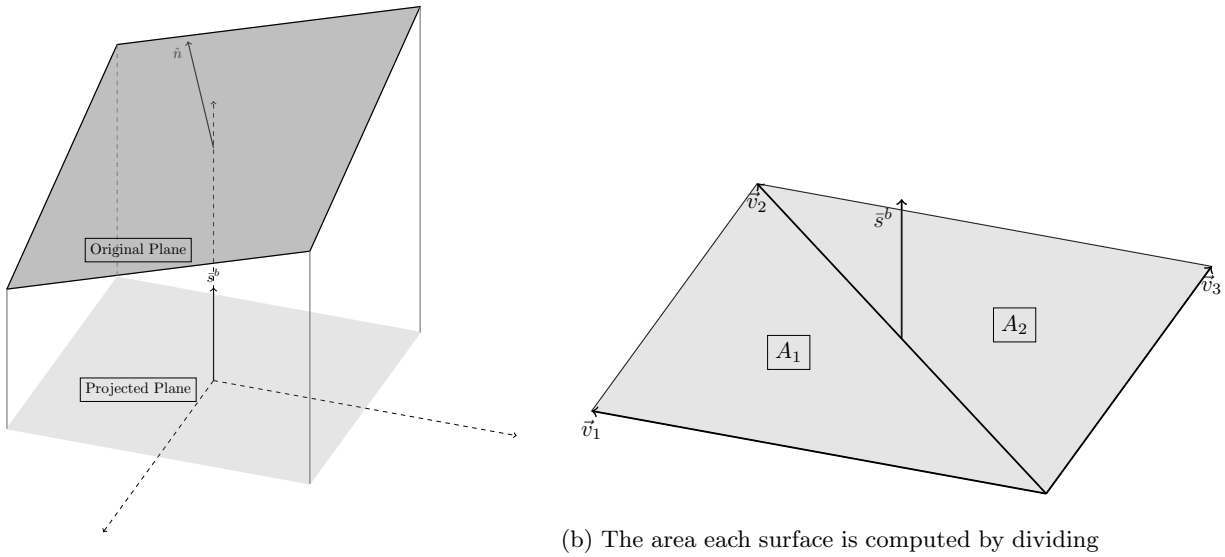

(a) Projection onto Sun plane.

(b) The area each surface is computed by dividing it into triangles as shown in the figure

FIG. 10: Schematic illustration of projection of the surfaces onto the Sun direction.

The area A_1 shown in the figure 10b can be computed as:

$$A_1 = \frac{1}{2} \left\| \vec{v}_1 \times \vec{v}_2 \right\|. \tag{A7}$$

Therefore, the total projected area can be computed as:

$$A_{tot} = \frac{1}{2} \sum_{i=1}^{n-1} \left\| \vec{v}_i \times \vec{v}_{i+1} \right\|. \tag{A8}$$

where n is the total number of corners. Dissecting each surface into triangles allows to compute each surface robustly. Moreover, in the preceding steps, Monte Carlo integration is performed in the shadowing algorithm, which requires to check if a given arbitrary point on $x' - y'$ is within a given area. This procedure can be much easily implemented for a triangular region. Monte Carlo integration requires the generation of large number of arbitrary points within a bounded domain[18]. In our problem, these points are generated within the bounding box of the projected plane formed by the corner points of the external surfaces of the satellite. Therefore, the bounding box is determined as:

$$x \in [\min(x'), \max(x')], \quad y \in [\min(y'), \max(y')] \tag{A9}$$

Here, the main objective is to compute the overlapping regions of each surface, as the areas of each projected surface can be computed as described above. If a given arbitrary point lies within an area enclosed by two separate surfaces, that points is on the region shadowed by the surface with larger z'. Finally, the ratio of the number of points within the overlap region shadowed by another surface to the total number of points within the area covered by the

DOI: 10.13009/EUCASS2019-910

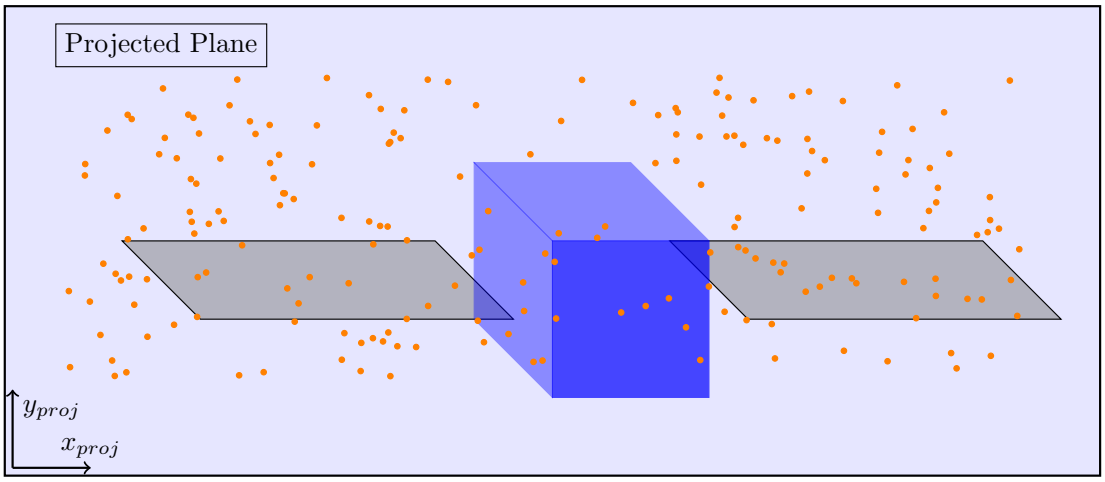

FIG. 11: Schematic View of Monte Carlo sampling in projected plane of a model satellite.

projection of that surface is approximately equal to the ratio of the shadowed area of that surface to the total area of that surface on the projected plane for large number of arbitrary points. To perform the Monte Carlo integration, $N = \mathcal{O}(10^5)$ number of random points are generated within the bounding box defined in equation A9. The points which lie within the overlapping regions shown schematically in figure 11 are first counted in each separate surface. Later, these surfaces are sorted with respect to their z' coordinate, the surface with the highest z' shadows the rest of the surfaces in the overlapping region. By Monte Carlo integration, the area of each projected surface can be obtained as:

$$A_j^N = A_{tot} \frac{1}{N} \sum_{i=1}^{N} f_j(x_i) \tag{A10}$$

where $f_j(x_i) = 0, 1$ and it checks if the point is inside the overlap region, A_j is the j_{th} overlapping region. Here, we define shadowing ratio as:

$$\gamma^k = \frac{A^k - A_j^k}{A^k} \tag{A11}$$

where k is the mesh number and A_j^k is the shadowed area of the mesh k.

[1] S.A. Billings. Identification of nonlinear systems–a survey. *IEE Proceedings D Control Theory and Applications*, 127(6): 272, 1980. ISSN 01437054. doi: 10.1049/ip-d.1980.0047. URL http://digital-library.theiet.org/content/journals/10.1049/ip-d.1980.0047.

[2] Steven L. Brunton, Joshua L. Proctor, and J. Nathan Kutz. Discovering governing equations from data: Sparse identification of nonlinear dynamical systems. volume 113, pages 3932–3937, 2015. ISBN 1091-6490 (Electronic) 0027-8424 (Linking). doi: 10.1073/pnas.1517384113. URL http://arxiv.org/abs/1509.03580{\%}0Ahttp://dx.doi.org/10.1073/pnas.1517384113.

[3] Steven L. Brunton, Joshua L. Proctor, and J. Nathan Kutz. Sparse Identification of Nonlinear Dynamics with Control (SINDYc). *IFAC-PapersOnLine*, 49(18):710–715, 2016. ISSN 24058963. doi: 10.1016/j.ifacol.2016.10.249. URL http://dx.doi.org/10.1016/j.ifacol.2016.10.249.

[4] Steven C. Chapra and Raymond Canale. *Numerical Methods for Engineers*. McGraw-Hill, Inc., New York, NY, USA, 5 edition, 2006. ISBN 0073101567, 9780073101569.

[5] Edgar Dachs and Artur Benisek. A sample-saving method for heat capacity measurements on powders using relaxation calorimetry. *Cryogenics*, 51(8):460 – 464, 2011. ISSN 0011-2275. doi: https://doi.org/10.1016/j.cryogenics.2011.04.011. URL http://www.sciencedirect.com/science/article/pii/S0011227511001196.

[6] D. Gamerman and F. L. Herbert. *Markov Chain Monte Carlo: Stochastic Simulation for Bayesian Inference*. Chapman and Hall/CRC, 2006.

[7] Freddy Alexander DÃaz GonzÃ¡lez, Pablo Roberto PinzÃCabrera, and Claudio Marcel HernÃ¡ndez CalderÃ. Design of a Nanosatellite Ground Monitoring and Control Software: a Case Study. *Journal of Aerospace Technology and Management*, 8:211 – 231, 06 2016. ISSN 2175-9146. URL http://www.scielo.br/scielo.php?script=sci_arttext&pid=S2175-91462016000200211&nrm=iso.

[8] Xu Guo-dong, Zhao Dan, Sui Shi-jie, and Lan Sheng-chang. Run-time control design of micro-satellite obc based on reconfigurable architecture. *2009 4th IEEE Conference on Industrial Electronics and Applications*, pages 2591–2595, 2009.

[9] Peter D. Hoff. *A First Course in Bayesian Statistical Methods*. Springer Publishing Company, Incorporated, 1st edition, 2009. ISBN 0387922997, 9780387922997.

[10] F.P. Incropera. *Fundamentals of heat and mass transfer*. Number v. 1 in Fundamentals of Heat and Mass Transfer. John Wiley, 2007. ISBN 9780471457282. URL https://books.google.com.tr/books?id=_P9QAAAAMAAJ.

[11] N. Iucci, A. E. Levitin, A. V. Belov, E. A. Eroshenko, N. G. Ptitsyna, G. Villoresi, G. V. Chizhenkov, L. I. Dorman, L. I. Gromova, M. Parisi, M. I. Tyasto, and V. G. Yanke. Space weather conditions and spacecraft anomalies in different orbits. *Space Weather*, 3(1):1–16, Jan 2005. ISSN 1542-7390. doi: 10.1029/2003SW000056.

[12] Henrik Wann Jensen and Niels Jørgen Christensen. Photon maps in bidirectional Monte Carlo ray tracing of complex objects. *Computers and Graphics*, 19(2):215–224, 1995. ISSN 00978493. doi: 10.1016/0097-8493(94)00145-O.

[13] Jung Hoon Kim and Byoungsoo Kim. Study on the reduction method of the satellite thermal mathematical model. *Advances in Engineering Software*, 108:37–47, 2017. ISSN 18735339. doi: 10.1016/j.advengsoft.2017.02.007.

[14] Jack K. Kreng, Michelle M. Ardeshiri, Oscar C. Barbosa, and Yogi Y. Krikorian. Telemetry, Tracking, and Commanding (TT&C) link considerations for a LEO Sat. *IEEE Aerospace Conference Proceedings*, 2005:1–10, 2005. ISSN 1095323X. doi: 10.1109/AERO.2005.1559457.

[15] A. Labibian, S.H. Pourtakdoust, A. Alikhani, and H. Fourati. Development of a radiation based heat model for satellite attitude determination. *Aerospace Science and Technology*, 82-83:479 – 486, 2018. ISSN 1270-9638. doi: https://doi.org/10.1016/j.ast.2018.09.031. URL http://www.sciencedirect.com/science/article/pii/S1270963818314159.

[16] Márcio Macedo and Antônio Apolinário. Improved anti-aliasing for Euclidean distance transform shadow mapping. *Computers and Graphics (Pergamon)*, 71:166–179, 2018. ISSN 00978493. doi: 10.1016/j.cag.2017.11.006.

[17] Maziar Raissi and George Em Karniadakis. Hidden physics models: Machine learning of nonlinear partial differential equations. *Journal of Computational Physics*, 357:125–141, 2018. ISSN 10902716. doi: 10.1016/j.jcp.2017.11.039. URL https://doi.org/10.1016/j.jcp.2017.11.039.

[18] Christian P. Robert and George Casella. *Monte Carlo Statistical Methods*. Springer Publishing Company, Incorporated, 2010. ISBN 1441919392, 9781441919397.

[19] F J T Salazar and O C Winter. Solar power satellite system in formation on a common geostationary orbit. *Journal of Physics: Conference Series*, 911:012006, oct 2017. doi: 10.1088/1742-6596/911/1/012006. URL https://doi.org/10.1088%2F1742-6596%2F911%2F1%2F012006.

[20] Robert P. Taylor, Rogelio Luck, B. K. Hodge, and W. G. Steele. Uncertainty analysis of diffuse-gray radiation enclosure problems. *Journal of Thermophysics and Heat Transfer*, 9(1):63–69, 1995. doi: 10.2514/3.629.

[21] Lloyd N. Trefethen and David Bau. *Numerical Linear Algebra*. SIAM, 1997. ISBN 0898713617.

[22] M. R. Vujičić, N. P. Lavery, and S. G.R. Brown. Numerical sensitivity and view factor calculation using the Monte Carlo method. *Proceedings of the Institution of Mechanical Engineers, Part C: Journal of Mechanical Engineering Science*, 220 (5):697–702, 2006. ISSN 09544062. doi: 10.1243/09544062JMES139.